



# Zein–Laponite nanocomposites with improved mechanical, thermal and barrier properties

Tahrima B. Rouf<sup>1</sup>, Gudrun Schmidt<sup>1</sup>, and Jozef L. Kokini<sup>1,\*</sup>

<sup>1</sup> Purdue University, 745 Agriculture Mall Drive, West Lafayette, IN 47907, USA

**Received:** 18 September 2017

**Accepted:** 22 January 2018

**Published online:**  
30 January 2018

© Springer Science+Business Media, LLC, part of Springer Nature 2018

## ABSTRACT

Zein, a prolamin of corn, is a bio-renewable resource that can potentially offer alternatives for petroleum-based polymers in many applications. Nanocomposite formation with the addition of silicate nanoparticles (Laponite) to zein films, cast from 70% ethanol solutions, significantly improved the mechanical, thermal and barrier properties. Based on FTIR findings, a mechanism for zein–Laponite nanocomposite formation is proposed, which suggests Laponite nanoparticles bind to zein molecules through Si–N bond formation. Structural characteristics investigated using AFM and TEM confirmed exfoliation of the nanoparticle. The changes in the surface energy of the films were evaluated using water contact angle measurements and showed an increase in surface hydrophobicity. The Young's modulus and tensile strength increased with nanoparticle concentration. The glass transition temperature increased, and water vapor permeability decreased with only a small amount of Laponite.

## Introduction

Petroleum-based polymers have exceptional physical and chemical properties including endurance and resistance to biological degradation. Unfortunately, these polymers are causing significant pollution and global environmental concerns [1]. For example, large plastic trash islands are floating on the oceans in many parts of the world [2], and plastic materials pollute pristine islands, lands and seas [3]. Therefore, biodegradable alternatives for plastics can solve some of these problems and improve environmental sustainability [4, 5].

The biopolymer zein is a major storage prolamin protein of corn and an abundant by-product of the ethanol industry. Zein is generally recognized as a safe (GRAS) material, by the Food and Drug Administration, and has unique amphiphilic, antioxidant, antibacterial and adhesive film-forming properties. Zein is considered a highly suitable candidate for designing environmentally friendly polymers [6–8]. The polymer chains of zein are able to change their conformation, and the mechanical and rheological properties can be tailored to give a range of properties from flexible to tough polymer, while maintaining a glossy appearance [9, 10]. Zein's versatile properties are useful for various applications in packaging, biomedical, agricultural areas and add

Address correspondence to E-mail: jkokini@purdue.edu

value to an abundant by-product of ethanol production. Zein has found applications in several industries including adhesives, coatings, printing, fibers, packaging films and plastics [11, 12].

Zein is an attractive alternative to synthetic polymers and animal-derived proteins, as zein has no allergenic compounds; it is a much less expensive and safe alternative for biomaterial research. When modified with different types of nanofillers, the resulting zein films showed significant improvements in mechanical, thermal, barrier and antimicrobial properties [7, 13–17]. Maximum improvement of zein properties is contingent upon optimum filler–matrix interaction, but the interaction between filler and zein matrix and the chemistry behind the property improvement of the matrices are not yet fully understood. In previous studies, where plasticized zein was reinforced with different nanomaterials [16, 18], proposed mechanisms suggested the supramolecular interaction between protein and reinforcing nanomaterials could result in cross-links that may reduce local mobility of the protein molecules. They then showed that these cross-links result in higher stiffness and glass transition temperature.

As efficient nanofillers, nanoclays have received a great deal of attention, as they are cost-efficient, chemically and thermally stable, and property enhancing due to their platelet-like structure. Laponite,  $\text{Na}_{+0.7}[(\text{Si}_8\text{Mg}_{5.5}\text{Li}_{0.3})\text{O}_{20}(\text{OH})_4]^{-0.7}$ , is a synthetic layered silicate nanoclay, which is hydrophilic and biocompatible [19]. Its well-defined nanosized disk shape has been used as a model in fundamental studies of polymer nanocomposites, to improve the mechanical and barrier properties [20–25]. These nanoparticles have also been studied for fabrication of sensors [26–28] and nanocomposite hydrogels [29, 30].

In our previous studies [8, 31, 32], zein has shown potential to be used in biodegradable packaging films, as well as microfluidic device and sensor platforms. Therefore, the aim of this paper is focused on the changes in mechanical, thermal, barrier and surface properties of zein, by the addition of Laponite. To investigate the effects of Laponite on zein, the changes in the physical properties and structural characteristics of the zein–Laponite (Z–L) nanocomposites were examined by changing the nanofiller concentration. Atomic force microscopy (AFM), transmission electron microscopy (TEM), water contact angle (WCA) measurements and Fourier

transform infrared (FTIR) spectroscopy were used to observe the structural changes occurring within the films when nanofillers were added. The effects of nanocomposite formation on mechanical, water vapor permeability and thermal properties are also presented. These experiments offer mechanistic insights into changes in physical properties of zein and show desirable results for use as a platform for biodegradable packaging, microfluidic devices, biosensor platforms and other functional film research.

## Experimental

### Materials

70% Ethanol (140 proof (70%), Decon™ Labs) and oleic acid were obtained from Fisher Scientific; monoglyceride was purchased from Alfa Aesar, Ward Hill, MA, USA; zein (90% crude protein dry weight basis) was purchased from Sigma-Aldrich, Milwaukee, WI, USA; and Laponite RD clay was obtained from Byk Chemicals. Drierites were purchased from W. A. Hammond Drierite Company. Polydimethylsiloxane (PDMS) kits were purchased from Sylgard, Dow Corning (Midland, MI).

### Fabrication of zein–Laponite nanocomposite films

A solvent casting technique was applied for preparation of the nanocomposite films, as it ensures optimal dispersion of the nanofillers and therefore ensures maximum interaction of the filler and matrix and use of environmentally preferred solvents [33]. Nanocomposite films (Z–L) were prepared with 0, 1, 3, 5 and 10 wt% Laponite, designated as Z–0L, Z–1L, Z–3L, Z–5L and Z–10L, respectively. First, the Laponite was dispersed in 25 mL of 70% ethanol/30% water and heated up to 60–65 °C. Then 5 g of zein was added to the solution (a 1:5 weight (g)/volume (ml) ratio was maintained) and stirred vigorously until the zein dissolved. In a separate beaker, 6.25 g of oleic acid plasticizer and 0.15 g of monoglyceride emulsifier were mixed and heated, until the monoglyceride dissolved in the oleic acid. The oleic acid–monoglyceride solution was added to the zein–Laponite solution, and the resulting mixture was stirred for another hour. The ratio of

zein/plasticizer/emulsifier (1/1/0.15) was maintained constant throughout this study because previous results showed that this formulation improved overall physical properties [32]. Prior to solvent casting each mixture was sonicated for at least 5 min with the sonicator amplitude set to 39% of total 500 watts. Ten milliliters of nanocomposite solution was pipetted into polystyrene petri dishes lined with PDMS, which allowed the zein film to be removed easily after solvent evaporation. The films were dried inside desiccators over calcium sulfate Drierite. The thicknesses of the dried films were fairly similar, and they were as follows: Z-0L =  $0.52 \pm 0.18$  mm, Z-1L =  $0.75 \pm 0.05$  mm, Z-3L =  $0.71 \pm 0.11$  mm, Z-5L =  $0.71 \pm 0.14$  mm, Z-10L =  $0.67 \pm 0.11$  mm.

### Characterization of nanocomposite films

#### *Transmission electron microscopy*

Transmission electron microscopy (TEM) was used to examine the structure of the Laponite nanoparticles and investigate the dispersion of the nanoparticles in the nanocomposite films. For nanocomposite sample preparation, the films were treated with fixative agents, followed by dehydration in an ethanol gradient. The films were embedded in epoxy resin, and then they were cut into ultra-thin sections using microtome diamond and mounted on holey copper grids. The microtomed samples were characterized with a Tecnai T20 TEM at 200 kV.

#### *Atomic force microscopy*

The surface morphologies and roughness of the nanocomposite films were investigated using a Veeco Multimode Atomic Force Microscope (AFM) (Veeco Instruments, Inc., New York). AFM tips used for characterization included a Si-Ni tip (spring constant: 37 N/m; frequency: 300 kHz), with a pyramidal shape and a height of 15  $\mu\text{m}$  (App Nano, Inc.). The film surfaces were imaged in the tapping mode and in scans of 500 nm  $\times$  500 nm according to the procedures published in the literature [34]. Data evaluation of images included calculating the average roughness (Ra) and the root-mean-square roughness (Rq).

#### *Fourier transform infrared spectroscopy*

Fourier transform infrared spectroscopy (FTIR) was performed for quantitative and qualitative analysis and for identifying specific chemical bonding within nanocomposites. Experiments were done using a nitrogen-cooled attenuated total reflectance FTIR (Nicolet Nexus 470 FTIR), with 64 scans at a resolution of  $4 \text{ cm}^{-1}$ . The spectra were recorded between 800 and  $4000 \text{ cm}^{-1}$ , and the spectra of water were subtracted before analysis to obtain only the protein spectrum [35]. For the secondary structure analysis of zein, deconvolution of each spectrum was done using the OMNIC FTIR software according to the methods of Fourier self-deconvolution (FSD). Three prominent and characteristic bands important for protein data evaluation are the amide I, II and III bands. The amide I band is a sharp peak that is usually seen between 1600 and  $1700 \text{ cm}^{-1}$  in protein spectra. This band is caused by the stretching of the C=O double bond and gives information about the secondary structures. The amide II and III bands are not analyzed here as they give peaks of weak intensity and can be easily overlooked [36]. The amide I regions ( $1600\text{--}1700 \text{ cm}^{-1}$ ) of the spectra were analyzed by Gaussian curve fitting. The secondary structural content was calculated from the relative areas of the individual assigned bands in the amide I region. The details of the curve fitting are included in the supplementary information.

#### *Differential scanning calorimetry*

DSC experiments were performed using a Discovery Nano Series DSC instrument. Calibration was based on pure indium and sapphire. An empty aluminum pan was used as reference. Samples of 10–14 mg were subjected to analysis using a heating rate of  $10 \text{ }^\circ\text{C}/\text{min}$  per heating cycle, under continuous purging of nitrogen at 50 ml/min. Glass transition temperatures were determined from resulting thermograms as the midpoint between onset and end temperatures of step changes in heat flow observed during heating. In all DSC traces, positive upward peaks correspond to exothermic processes and downward peaks correspond to endothermic processes.

### Water vapor permeability

The barrier properties of the nanocomposite films were analyzed using water vapor permeability (WVP) experiments. WVP cups were purchased from the Paul N. Gardner Company, Inc., and measurements were taken using an American Society for Testing and Materials, ASTM E-96 (1996), standard [37]. The zein-Laponite (Z-L) films were attached to the permeability cups containing 8 mL of distilled water. Then the cups were placed in desiccators containing a saturated salt solution of  $\text{MgCl}_2$ , while a temperature of 22 °C and a relative humidity (RH) gradient of 64% were maintained. The sample cups were weighed every 24 h until steady-state vapor flow was reached. At least three sets were tested for each formulation. The water vapor transmission rate was calculated from the weight loss of the permeation cup. The water vapor transmission rate (WVTR) was defined as the slope (g/hr) divided by the transfer area ( $\text{m}^2$ ). After the permeation tests were completed, the water vapor permeability, WVP ( $\text{g Pa}^{-1} \text{h}^{-1} \text{m}^{-1}$ ), was calculated as follows:

$$\text{WVP} = \frac{\text{WVTR}}{P(R_1 - R_2)} \times x, \quad (1)$$

where  $P$  is the saturation vapor pressure of water (Pa) at the test temperature (25 °C);  $R_1$  is RH in the permeation cell;  $R_2$  is the RH in the  $\text{MgCl}_2$  solution; and  $x$  is the film thickness (m).

### Water contact angle measurements

Water contact angle measurements were taken with an Attension Theta Auto 1 Optical Tensiometer. All measurements were taken on the sides of the zein-Laponite films that were previously in contact with PDMS. Two-microliter droplets of deionized water were dispensed onto the surface of the film, and images were collected for 10 s at a rate of 12 frames per second. The images were taken as soon as the water droplet touched the designated baseline. Then the stable contact angle at the water zein film interface was measured and the change in hydrophobic/hydrophilic balance on film surfaces was evaluated. Water contact angle measurements were taken in triplicate for the contact side, following the method described in the literature [38].

### Mechanical properties

The tensile strength (TS), Young's modulus (YM) and percentage of elongation at break (% EAB) of films were determined using a TA. XT Plus Texture Analyzer with a 30 g load cell using ASTM D882 [39]. The films were cut into 20 mm × 70 mm strips, and the samples were kept for 48 h at 50% relative humidity and 25 °C before analysis. Three thickness measurements were taken across the gauge length of the films and averaged. The pretest and posttest speed was 1 mm/min.

### Statistical analysis

For each of the five-different zein nanocomposite formulations, the experiments were repeated three times. Data were statistically analyzed and compared using Minitab. One-way ANOVA was used to evaluate the differences, and Tukey's pairwise comparison tests were applied with 95% confidence interval. The letter system was used throughout the paper to show significant difference such that different letters indicate significant difference between the adjacent values.

## Results and discussion

### Transmission electron microscopy

An important prerequisite for the improvement of the physical and mechanical properties is the uniform nanoparticle dispersion within the nanocomposite. TEM provides information about the dispersion of the Laponite and therefore helps explain the physical changes as a result of the nanoparticle–matrix interactions. In order to baseline the organization of Laponite, 1 g Laponite powder has been mixed with 10 mL of 70% aqueous ethanol solution, stained with 1% uranyl acetate and imaged with TEM, and is shown in Fig. 1a. Light-colored streaks that are prevalent throughout the image are on average 1 nm thick and 25 nm long. These streaks represent the side view of individual Laponite nanoparticles. As Laponite is disk shaped, the appearance of these streaks means that some Laponite nanoparticles are arranged perpendicularly to the surface so that only the side view of the disks can be seen. The top view of nanoparticles that may lie flat on the surface cannot

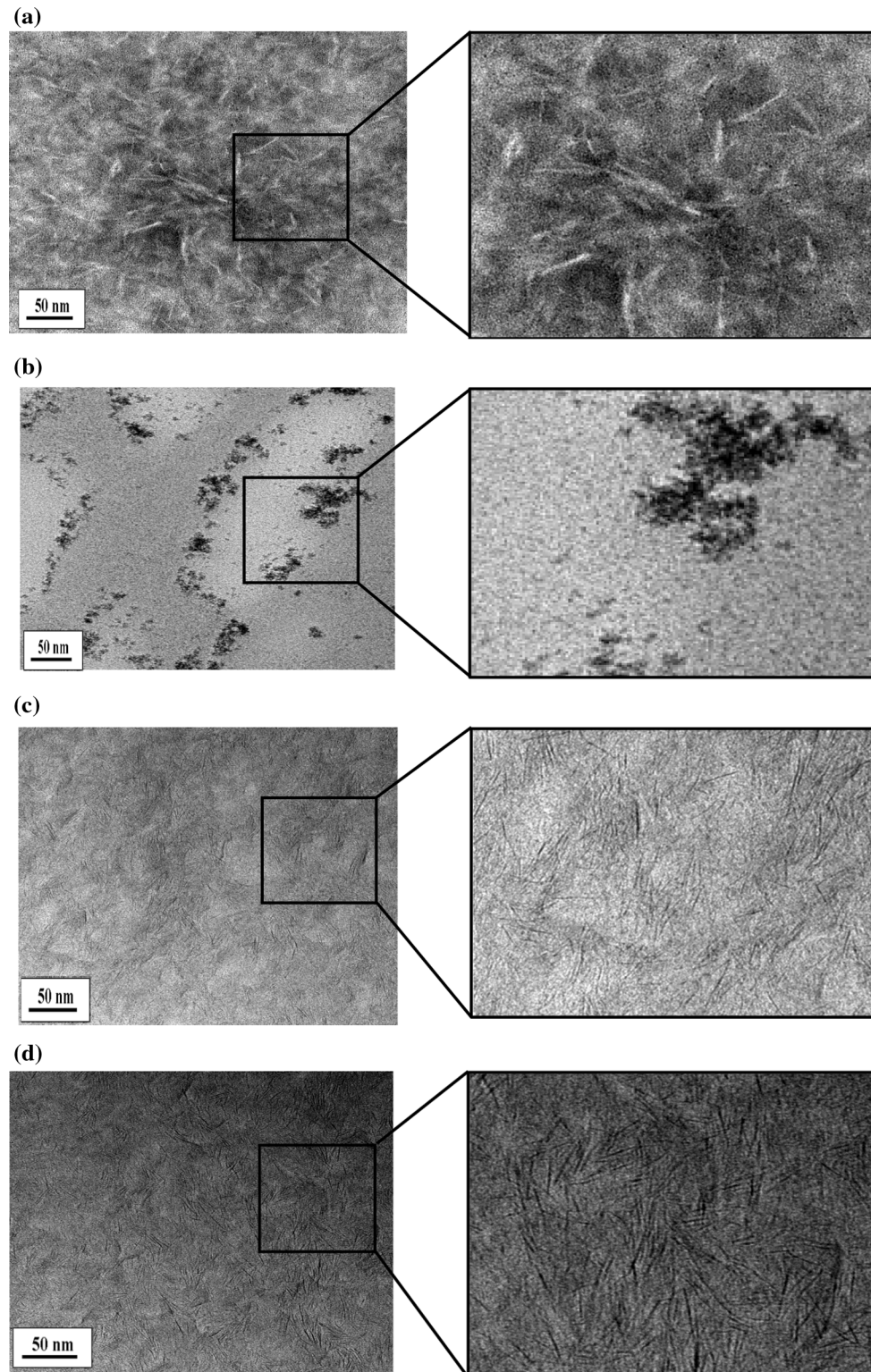


**Figure 1** TEM images: **a** pristine Laponite nanoparticles can be recognized as white streaks against the dark background (stain: uranyl acetate). The magnified areas show more details. **b** Plasticized zein film showing dark areas of phase-separated oleic acid. **c** Z-5L nanocomposite film, showing intercalated, exfoliated

Laponite platelets dispersed throughout the zein matrix. **d** Z-10L nanocomposite film, showing intercalated, exfoliated Laponite platelets and some degrees of aggregation. The magnified areas show individual nanoparticles as seen from the side.

be seen here due to low contrast. The top view of individual Laponite nanoparticles can be seen in published work, for example, by Guimarães et al. [40]. In this paper, formation of Laponite-covered latexes allows the nanoparticles to be imaged from the top so that the coin-like shapes can be seen. However, in the case of solution casting presented here, the nanoparticles align sideways; therefore, only streaks are observed in the TEM (Fig. 1a, c, d).

Figure 1b shows the TEM image of a zein film containing oleic acid plasticizer. The dark spots seen within the polymer matrix come from phase-separated oleic acid. Figure 1c, d shows images from zein–Laponite nanocomposites. The dark streaks represent Laponite nanoparticles as seen from the side. The Laponite is homogeneously dispersed, but visible throughout the zein matrix. Single platelets can be observed together with stacked and multi-layered nanostructures within the zein matrix. The images suggest that Laponite is exfoliated (individual platelets fully separated) to some degree, but also intercalated (partially separated individual platelets) areas are visible. As the concentration of Laponite increases to 10% (Fig. 1d) intercalated areas are more frequent and aggregation becomes more pronounced. Within small aggregates or domains, the nanoparticles appear to align parallel to each other. This parallel orientation or intercalation is more prominent at higher Laponite concentrations where polymer space decreases and a house of cards structure is not feasible any more. Intercalation and orientation of Laponite within smaller domains further increases barrier properties, and thus, water vapor permeability decreases (see below). The structural characteristics observed here can be related to the sample preparation and film casting techniques used.

Figure 2 shows photographs of the three different nanocomposite films taken over a Purdue Pete cartoon, to examine the optical appearance of the films. The zein control (Z–0L) is yellow but transparent to the eye. With increasing Laponite content the cartoon is still visible through films (Z–5L) and (Z–10L) even at the highest loading of (10 wt%) Laponite. However, the yellow (Z–10L) film appears to be darker and perhaps not as clear as the zein control when examined by the eyes. This means that Laponite may have some influence on the optical appearance of the films. We assume that at the concentrations used here, most of the nanoparticles are exfoliated or intercalated (see Fig. 1); however, micron-sized

heterogeneities in the films or density fluctuations of Laponite within the polymer matrix (see, TEM, Fig. 1) may lead to darker and translucent films.

### Atomic force microscopy

Atomic force microscopy (AFM) is another technique that helps visualize and understand the dispersion of the nanoparticles, as uniform dispersion can lead to smoother surfaces compared to the original polymer matrix [41]. Non-uniform dispersion can lead to rough and irregular surface properties [25]. As uniform dispersion leads to better interactions between polymer and nanoparticles, the AFM technique also helps optimize the fabrication of better nanocomposite films with improved properties. Surface topography of Laponite nanoparticles using AFM has been investigated in different studies [42–44], and in those studies, the nanoparticles have shown characteristic rag-like surface with domains of ridges and valleys. Topographies of the zein control (only plasticized) and zein–Laponite nanocomposite surfaces are shown in Fig. 3. The images shown in Fig. 3a, b suggest that pristine zein surfaces have high surface roughness which is in agreement with findings from the literature [34, 45]. Figure 3c, d displays the surface topology of a representative zein–Laponite nanocomposite (Z–5L). Comparison of Fig. 3a, c, shows that the control zein film has large features and bumpy areas with cavities, whereas the Z–5L nanocomposite films have isolated small granular-like domains [46]. The surface topography of the nanocomposite resembles the surface topographies of pristine Laponite nanoparticles [44], as the nanocomposite films also seem to have a rag-like structure.

‘Roughness analysis’ for the control zein films yields an average roughness of  $R_a = 5.83$  nm and a root-mean-square roughness of  $R_q = 7.11$  nm. Analysis of Z–5L, the 5% Laponite containing nanocomposite, gives  $R_a = 0.567$  nm and  $R_q = 0.799$  nm. These results indicate that Laponite disperses well within the zein matrix, thus creating a smoother surface. The dispersion of the Laponite and the nanoparticle interactions with the zein polymer influence the arrangement of the polymer chains near the Laponite surfaces, which results in a more compact structure. With increasing Laponite concentration (Z–5L), the amount of zein in the matrix decreases, which leads to a change in the surface

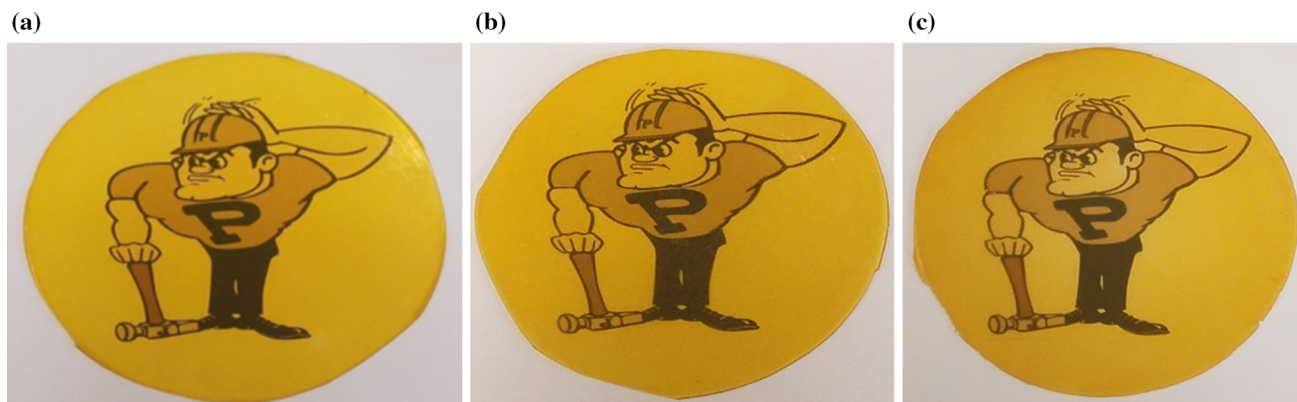


**Figure 2** Photographs of zein control and zein–Laponite films over the Purdue Pete cartoon as they appear to the eye. **a** Z–0L film, **b** Z–5L film and **c** Z–10L nanocomposite film.

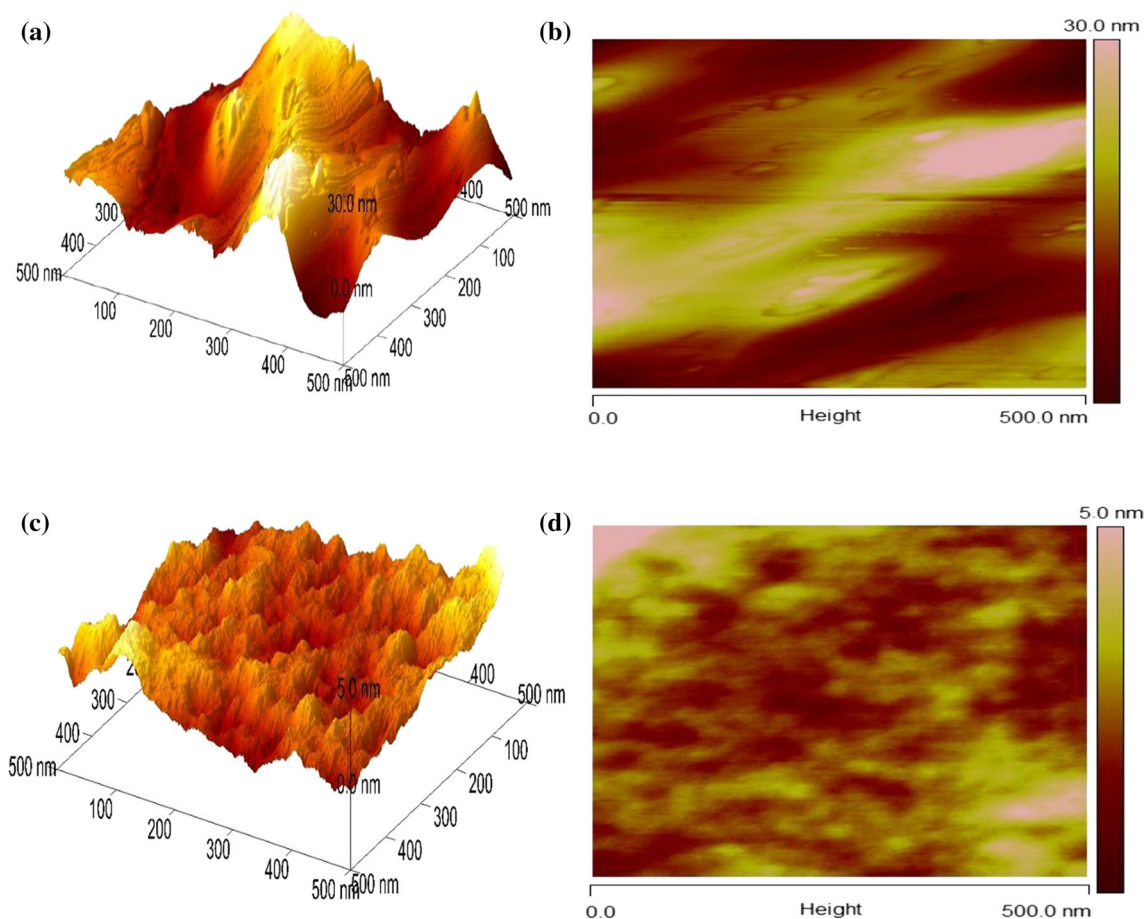


**Figure 3** **a** Three-dimensional AFM image of a control zein film on a 500 nm × 500 nm scale, showing large features as high as 30 nm. **b** Top view of the control zein film section. **c** Three-

dimensional image of a Z–5L film on a 500 nm × 500 nm scale, showing smaller granular areas. The height of the features is as high as 5 nm. **d** Top view of the Z–5L film section.

roughness when compared to the zein-only control. This change in surface roughness is influenced by the degree of exfoliation and intercalation of the Laponite, throughout the zein matrix.

Other studies investigating Laponite nanocomposite surfaces have reported slight increases in roughness [25], mostly due to irregular or non-uniform dispersion of the nanoparticle in the polymer

matrix. Publications on different polymer–clay nanocomposites such as chitosan–montmorillonite [41] or poly(3-hydroxybutyrate-co-3-hydroxyvalerate)–Cloisite 30B [47] have reported significant decreases in surface roughness after addition and dispersion of clay.

### Fourier transform infrared spectroscopy

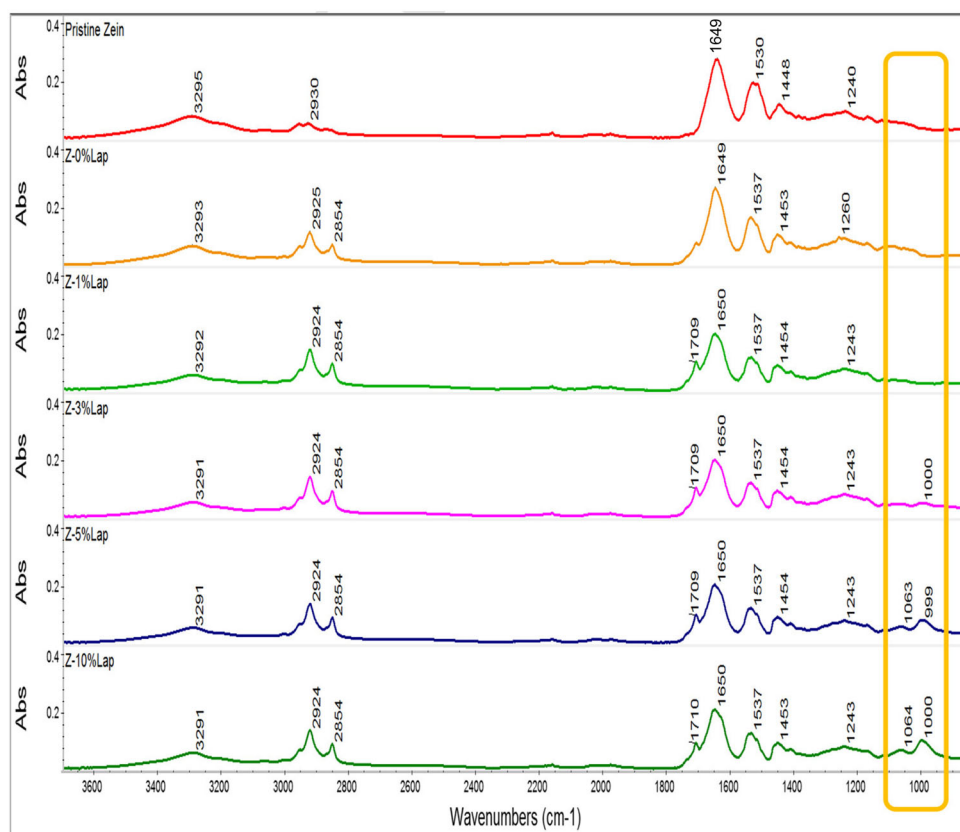
In Fourier transform infrared spectroscopy (FTIR), the rise of new peaks or the shift in original peaks may give information about the physicochemical environment of functional groups within the nanocomposite. The changes may confirm specific interactions between the polymer matrix and the nanoparticles, which in turn helps understand and improve nanocomposite material design. Figure 4 shows the FTIR data from pristine zein powder, plasticized control zein films and plasticized nanocomposite films containing 1, 3, 5 and 10% Laponite. FTIR data of pristine zein powder and the zein control and nanocomposite films show the typical characteristics of proteins including the amide I, II and III bands or peaks. The peaks observed

between 2800 and 3000  $\text{cm}^{-1}$  come from  $-\text{CH}_3$  and  $-\text{CH}_2$  side chain vibrations in aliphatic groups of amino acids. The broad peak at 3000–3500  $\text{cm}^{-1}$  is related to the N–H stretching in amide structures [48]. The amide I band at 1643  $\text{cm}^{-1}$ , which comes from C=O and C–C vibrations, and the amide II band at 1536  $\text{cm}^{-1}$ , related to CN stretching and NH bending, are visible [48].

When pristine zein is compared to the control zein plasticized with oleic acid, an increase in intensity is visible at 2924 and 2854  $\text{cm}^{-1}$ . The oleic acid increases the number of alkyl groups in the matrix; these alkyl groups show C–H stretching vibrations in the FTIR. Therefore, the presence of additional alkyl groups from the oleic acid plasticizer resulted in increased C–H stretching [48] and ultimately increased the intensities of the peaks at 2924 and 2854  $\text{cm}^{-1}$ . A new peak at 1709  $\text{cm}^{-1}$  comes from the carboxylic C=O stretching of the oleic acid.

Typical FTIR spectra of pristine Laponite show a prominent peak from Si–O stretching, located at 1080  $\text{cm}^{-1}$  [49]. The Si–O peak has also been located at 1011  $\text{cm}^{-1}$  [50] and at 1090  $\text{cm}^{-1}$  [38]. A comparison of the FTIR spectra in Fig. 4 shows the rise of

**Figure 4** Comparison of the FTIR spectra of pristine zein powder, control zein with oleic acid and zein–Laponite nanocomposites (1, 3, 5 and 10%), within the 3700–800  $\text{cm}^{-1}$  range. Addition of oleic acid results in increases in the intensity of new peaks at 1709  $\text{cm}^{-1}$  due to the carboxylic acid C=O stretch and at 2854  $\text{cm}^{-1}$  due to alkyl C–H stretch, and further addition of Laponite results in new peaks at 1064  $\text{cm}^{-1}$  which can be attributed to Si–O stretching. The peak at 1000  $\text{cm}^{-1}$  can be attributed to Si–N stretching.





new peaks at  $1000\text{ cm}^{-1}$  for Z-3L, Z-5L and Z-10L, and at  $1064\text{ cm}^{-1}$  for Z-5L and Z-10L, which is similar to the peak found in Laponite at  $1080\text{ cm}^{-1}$  (Si-O). The multiple spectra obtained for each concentration of Laponite were averaged over multiple locations. They are reproducible and superimpose nicely indicating that on average, the Laponite has been distributed uniformly throughout the zein matrix. This is consistent with our observations with TEM. The gradual increase in intensity of the new peaks indicates a gradual increase in nanoparticle concentration.

The chemical changes observed in FTIR are related to the addition of Si-O groups and may affect the secondary structures of zein. Within the amide I band, the  $\alpha$ -helix structures give characteristic peaks around  $1653\text{--}1658\text{ cm}^{-1}$ , the  $\beta$ -sheets give characteristic peaks around  $1632\text{--}1636\text{ cm}^{-1}$ , and the  $\beta$ -turn structures show characteristic peaks around  $1680\text{--}1686\text{ cm}^{-1}$  [51]. Another study [52] has reported that  $\beta$ -turns appear around  $1671\text{ cm}^{-1}$  and intermolecular  $\beta$ -sheets appear around  $1610\text{ cm}^{-1}$ . Pristine zein, Z-0L–Z-10L, nanocomposites show  $\beta$ -turns,  $\alpha$ -helices, as well as intramolecular and intermolecular  $\beta$ -sheets. The nanocomposite formation affected the area and height intensities of all the characteristic amide I peaks. From Fig. 5 we can conclude that the area under the peak that is related to  $\beta$ -sheets increases relative to the control. The area under the peak related to  $\alpha$ -helices decreases with increasing Laponite concentration, and the  $\beta$ -turns

remain the same. The formation of new bonds between Si-O and zein eliminates some of the degrees of freedom that the conformation of zein had before being absorbed to the Laponite surfaces. The change in degree of freedom explains why the zein molecules become more rigid with an increase in  $\beta$ -sheet conformation, and this transformation occurs at the expense of  $\alpha$ -helices.

Zein organizes itself in mostly compact capsule-like structures which are bonded to each other through glutamine residues [53].  $\beta$ -turns are largely associated with the glutamines at the end of the capsule-like bodies, and since their ratio remains the same, the glutamines are not affected by the bonding processes through Si-O.

It is reasonable to expect that Laponite can interact with zein in two ways: either through glutamine ends of zein, or the Si-O interacts with the N atom in the hydrophobic alpha helices, and forms a bond. Since  $\beta$ -turns show no change with the addition of Laponite in Fig. 5, it can be assumed that Laponite does not bond with zein through glutamine turns. A mechanistic figure depicting the possible interaction sites between zein and Laponite is shown in Fig. 6.

As suggested in Fig. 6, a logical way is that the Si-O group of Laponite breaks up the H bond in the  $\alpha$ -helix and forms either Si-C or Si-N bonds, which results in changing of the  $\alpha$ -helix into  $\beta$ -sheets, or  $\beta$ -turns. The rise of a new peak at  $1000\text{ cm}^{-1}$  as shown in Fig. 4 can be attributed to Si-N stretching [54–56]. The characteristic peak at  $800\text{ cm}^{-1}$  for Si-C [57] is

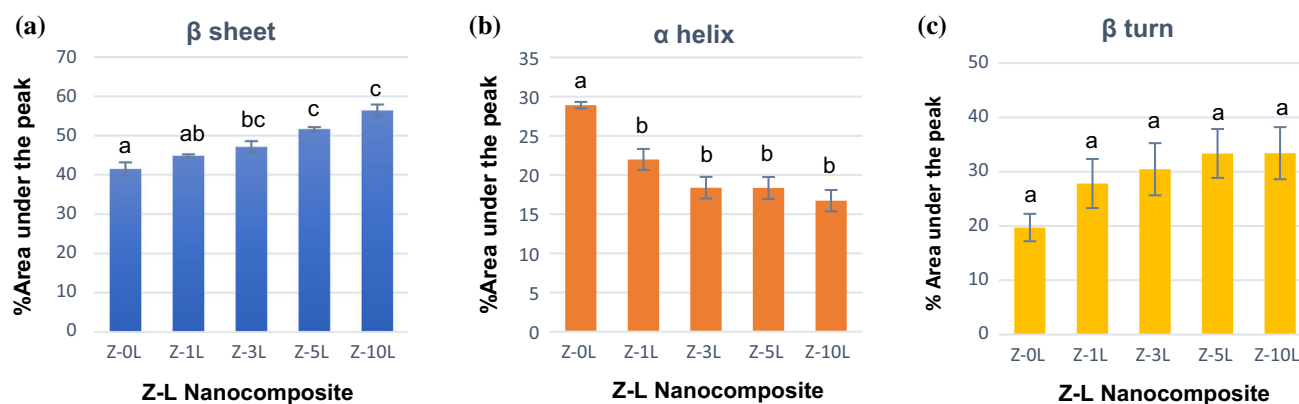


**Figure 5** Comparison of change in secondary structure distribution, in the amide I region, with the addition of Laponite. **a**  $\beta$ -sheet shows increase, **b**  $\alpha$ -helix shows decrease, and **c**  $\beta$ -turns show increasing trend, indicating that the addition of Laponite to zein promotes the decrease in ordered structure and gives rise to more disordered structure. Different letters above error bars signify

statistically significant differences according to Tukey's pairwise comparison ( $p < 0.05$ ). Although the area under the peak shows an increasing trend for  $\beta$ -turns, the standard deviation is high. Therefore, these data points are not considered significantly different by Tukey's pairwise comparison. Therefore, the columns for  $\beta$ -turns have the same letter above them.

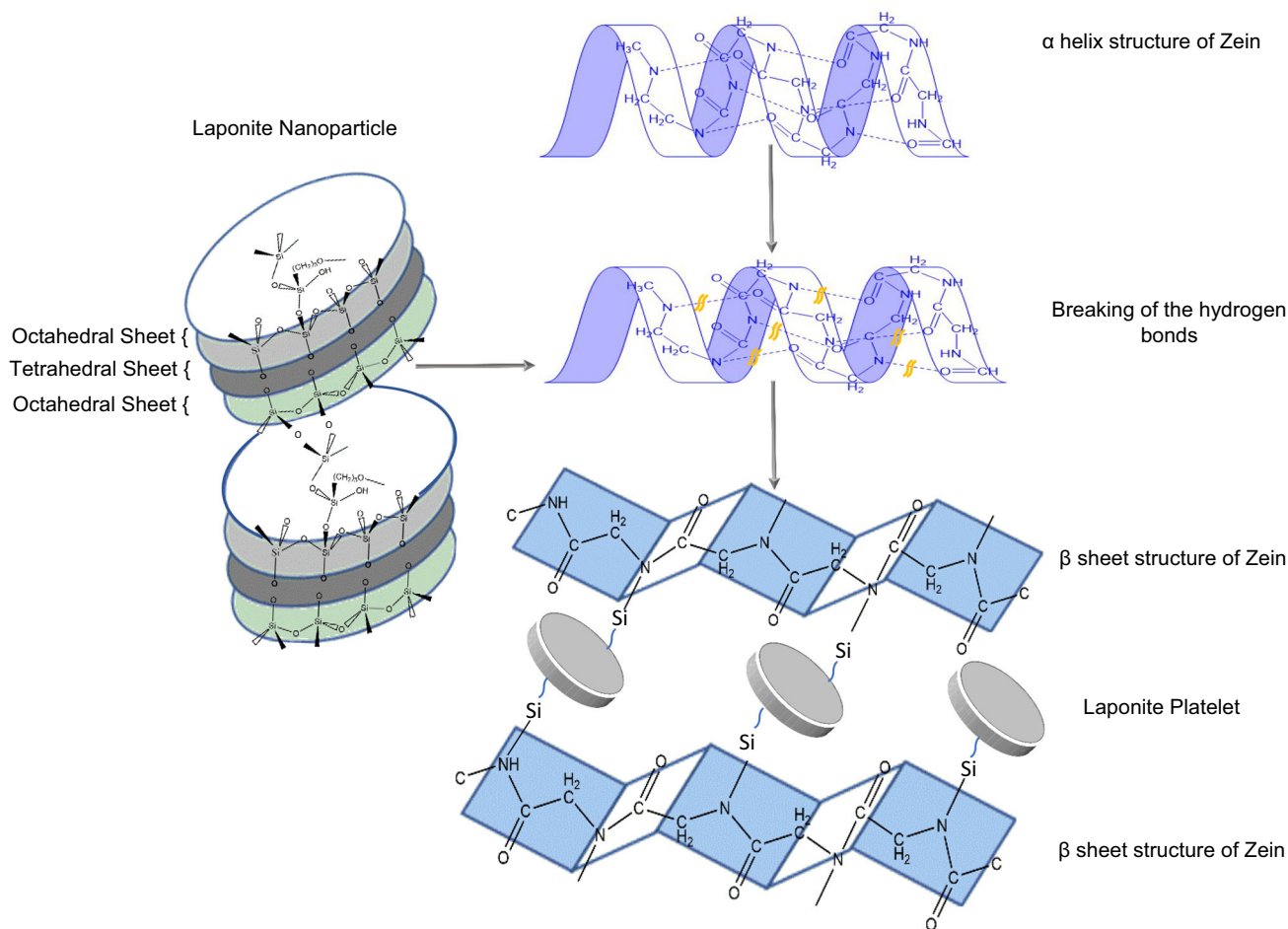


**Figure 6** Proposed mechanism of interaction between zein and Laponite.

not observed, leading to the conclusion that no Si–C bonds were formed.

### Differential scanning calorimetry

The differential scanning calorimetry (DSC) gives information of the changes in the thermal properties of the nanocomposites, which can be a direct result of the interaction and physical or chemical bond formation between the polymer matrix and nanoparticles. In Fig. 7a, the DSC thermograms of the zein–Laponite nanocomposites shifted (right) to higher temperatures with increasing Laponite content and the glass transition temperature  $T_g$  showed an increase with increasing Laponite content. This is also clearly shown in the histograms in Fig. 7b. The increase in  $T_g$  is probably due to the higher restricted chain mobility resulting from the interactions of Laponite and the zein polymer chains. This result confirms the FTIR findings, which show that the

formation of new bonds between Laponite Si–O and zein eliminates some of the degrees of freedom of the conformation of zein. Interactions with Laponite make zein more rigid, resulting in an increase in  $\beta$ -sheet conformation and a decrease in  $\alpha$ -helices. This result is also in good agreement with mechanical properties, which show higher tensile strength with increasing Laponite content.

Other studies showed that the addition of Laponite as well as other clays like montmorillonite increases the  $T_g$  of PMMA [58]. Similar results were reported by Manisara and Pancheri, where they found that the addition of cellulose microfibrils to zein increased the  $T_g$  of zein films [15]. Other biopolymer–nanocomposite studies show a similar trend of nanofillers bonding with polymeric chains, thereby creating a more compact and rigid structure, which increases the  $T_g$ . This increase correlates with the tensile strength and Young's modulus and with a decrease in the % elongation at break [59].

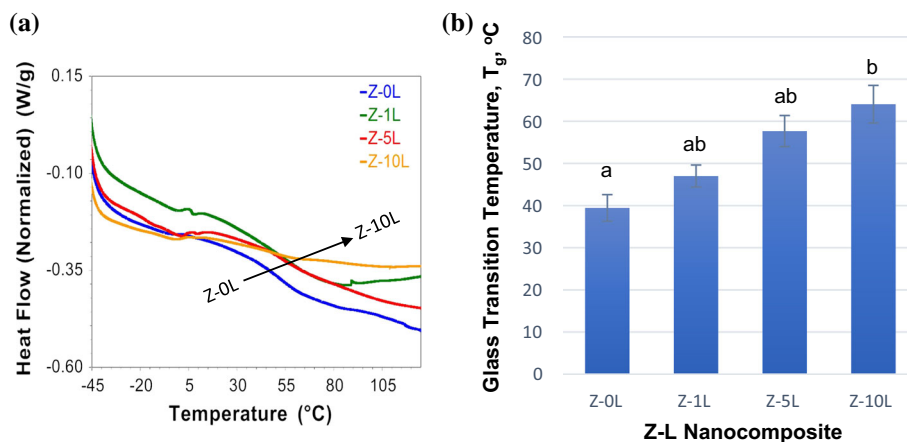


**Figure 7** a DSC thermograms of zein–Laponite nanocomposites. b DSC histograms of zein–Laponite nanocomposites. Addition of Laponite increases the glass transition temperature, indicating that

### Water vapor permeability

The water vapor permeability (WVP) is an important property that guides the application of the biopolymer. An increase in permeability is sometimes desired, for example, for wound dressings [60], whereas in some cases a decrease in WVP is crucial for applications such as biosensors and packaging materials. WVP of zein–Laponite nanocomposite films is shown in Fig. 8. The data suggest that the WVP decreased as the Laponite content increased up to Z-10L. The WVP decreased the most (about 40%) for Z-10L. It appears that the influence on barrier properties has a linear relationship with Laponite content. The improvement of water vapor barrier

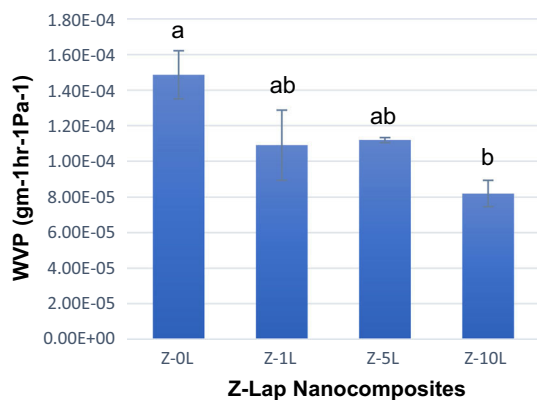


**Figure 8** Water vapor permeability decreased with increasing Laponite concentration, indicating that the presence of Laponite in the zein polymer matrix creates a tortuous path for the water molecules to escape. Different letters above error bars signifies a statistically significant difference ( $p < 0.05$ ).

Laponite forms a bond with zein polymer chains and increases rigidity, and hence raises  $T_g$ . Different letters above error bars signify a statistically significant difference ( $p < 0.05$ ).

properties of Z–L nanocomposite films is due to the presence of impermeable Laponite platelets that are distributed in the polymer matrix in a manner that increases the effective diffusion path length. The level of improvement depends not only on the nanocomposite structure (intercalated, exfoliated or some intermediate), but also upon the relative orientation of the sheets or nanoplatelets in the matrix. The Laponite orientation can result in highest tortuosity when the nanoplatelets arrange perpendicular to the direction of diffusion. Any kind of deviation from such an arrangement results in an increase in WVP. From the TEM images shown in Fig. 1, we can see that on average the nanoplatelets are randomly oriented. However, within small aggregates or domains the nanoplatelets are not exfoliated, but remain intercalated. Parallel orientation or intercalation of Laponite within small domains further increases barrier properties through creating a tortuous path for small water molecules. This effect can be observed when comparing water vapor permeability data of Z-5L and Z-10L in Fig. 8.

### Water contact angle measurements

Several studies from the literature report a relationship between water contact angle measurements and water vapor permeability [61–64]. The authors usually find that an increase in hydrophobicity leads to an increase in water vapor barrier properties. One explanation for such behavior is that polar  $\text{H}_2\text{O}$  molecules cannot be readily adsorbed to nonpolar film surfaces or hydrophobic surfaces, which

ultimately results in a reduction in water vapor permeability. Since Laponite is hygroscopic as well as hydrophilic, we would assume that the addition of Laponite will increase the hydrophilicity of a polymer nanocomposite, which in turn may reduce the barrier properties of the film. Here we investigate the surface hydrophilicity by presenting water contact angle measurements (WCA) on zein–Laponite surfaces. We then determine how the changes in WCA are correlated to the WVP findings presented above.

Water contact angle, WCA, measurements were taken from the zein–PDMS contact side. Figure 9 shows the average WCA values for films with different Laponite concentrations. The control zein and the Z–L nanocomposites showed hydrophilic properties, as their WCA was lower than 90°. Control zein had a contact angle of 54° which is consistent with the findings from the literature [38]. However, as Laponite was added to zein, the WCA started to increase; the highest WCA recorded was  $64.77 \pm 1.76^\circ$  for Z–5L nanocomposite. Surprisingly, Laponite addition slightly increased the hydrophobicity, by increasing the WCA. The change in the WCA with different concentrations of Laponite can be the function of surface morphology of the films, coating of the Laponite with zein polymer and orientation of the nanoparticle in the nanocomposite. Similar results were found for montmorillonite clay, MMT, which increased the water contact angle of methyl cellulose [65] and regenerated cellulose [66] nanocomposites. Another study on Cloisite 10A, a hydrophilic

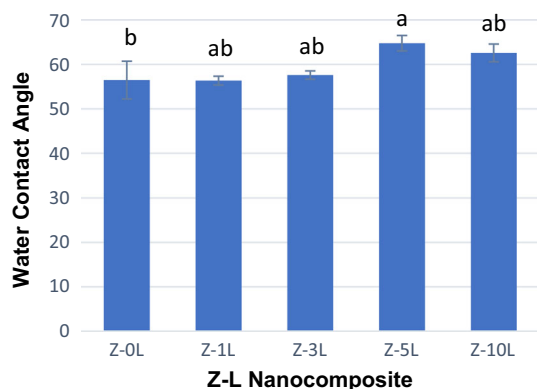


**Figure 9** Water contact angle of zein–Laponite nanocomposites shows an increase with increasing Laponite concentration. The presence of Laponite slightly increases the hydrophobic properties of zein. However, the WCA of the nanocomposite films is still within hydrophilic range. Different letters above error bars show statistically significant differences ( $p < 0.05$ ).

nanoclay, and zein also showed an increase in WCA [17]. Our data suggest that the increasing amount of zein-covered Laponite surfaces prevented the spreading of the water droplets and increased the WCA. This may be correlated to the formation of hydrophobic Si–N groups (Si from Laponite; N from amide) on the surface, which is supported by the FTIR results (Fig. 4). As the degree of surface hydrophobicity increased, the WVP of nanocomposite films decreased. This trend may indicate a relationship between contact angle changes and water vapor barrier due to the presence of Laponite in the polymer matrix.

### Mechanical property

Mechanical properties of nanocomposites constitute an important factor in its various biomaterial applications. Nanocomposites should withstand different stresses, whether used as microfluidic substrates, as scaffolding materials or in food packaging. The mechanical properties of zein–Laponite nanocomposites including tensile strength (TS), Young’s modulus (YM) and % elongation at break (EAB) are shown in Fig. 10. With increasing Laponite concentration the tensile strength and the Young’s modulus increased, while the elongation at break decreased. The Z–L nanocomposite films had greater Young’s modulus and tensile strength than the pristine zein films. The tensile strength which is the maximum tensile stress that the sample can carry before rupture improved the most for Z–10L. The tensile strength of the pristine zein control was  $2.26 \pm 0.48$  MPa and increased to  $5.53 \pm 0.17$  MPa when 10% Laponite was added (Z–10L). This corresponds to a 150% increase in tensile strength. The Young’s modulus, YM, increased from  $41 \pm 1.9$  MPa (Z–0L) to  $114 \pm 7.8$  MPa (Z–10L), which corresponds to a 180% increase. The elongation at break, EAB, decreased with increasing Laponite concentration. The reason behind the decrease in EAB with increasing Laponite concentration can be attributed to the Si–N and Si–O bond formation (as seen in FTIR results), due to the interaction between the zein polymer and Laponite nanoparticles. Increasing Laponite particles increased the number of bond formation; as a result, the polymer chain experiences restricted mobility and % elongation at break decreased.

In Table 1, Comparison with property modification of other zein nanocomposite films from the literature

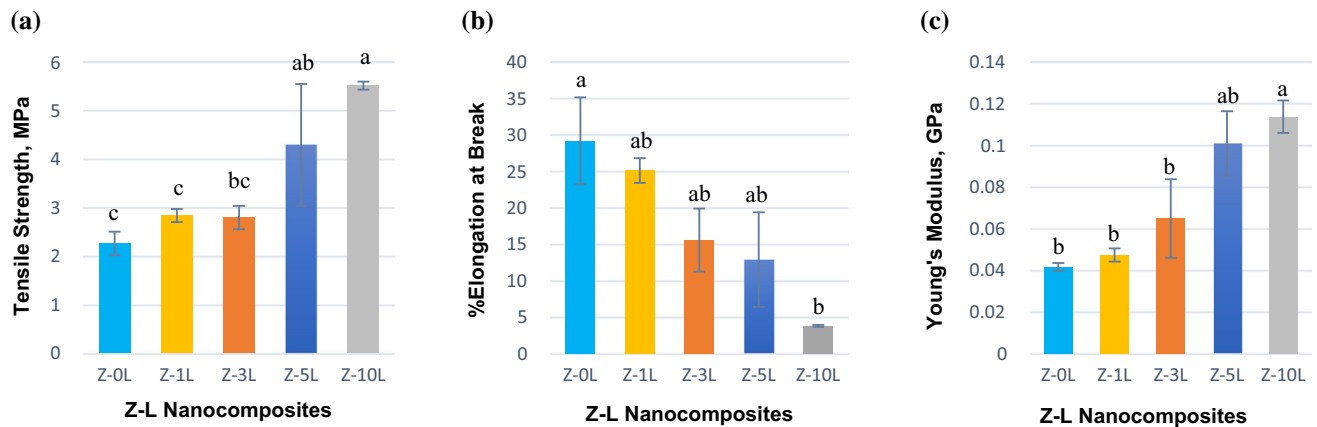


**Figure 10** Comparison of the different mechanical properties of the zein–Laponite nanocomposites: **a** tensile strength, **b** %elongation at break, **c** Young’s modulus. Different letters above error bars signify a statistically significant difference ( $p < 0.05$ ).

**Table 1** Comparison of mechanical property modification of different zein nanocomposites (with similar %nanomaterial loading) from the literature

Zein treatment	Plasticizer	% Nanofiller	Tensile strength		Young’s modulus		Refs.
			% Increase	Value (MPa)	% Increase	Value (MPa)	
L	Oleic acid	5	↑90%	4.3	↑146%	101	Current study
MMT	PEG	5	↑127%	6.48	↑ 315%	3.36	[7]
CMF	Glycerol	4	↑28%	15.05	↑62%	14.75	[15]
AL	Polyethylene glycol	5 (1)*	↑153%*	3.8 (4.53)*	NA	NA	[16]

L Laponite, MMT montmorillonite, CMF cellulose microfibrils, AL alkaline lignin

\*Zein–AL nanocomposite showed highest tensile strength at 1% loading, but then it started to deteriorate, so tensile strength results for both 1 and 5% loading are reported

shows that the Z–L nanocomposites had the highest Young’s modulus improvement compared to the other nanocomposites of zein.

### Conclusion

For this study, novel biodegradable zein–Laponite nanocomposites were successfully engineered, aiming at understanding the chemistry behind zein–Laponite interaction, for advanced material design. Different fractions of Laponite were incorporated into the zein biopolymer matrix using solvent casting technique, and their investigation focused on the effects of Laponite concentration on the mechanical, thermal, barrier and other physical properties, using the AFM, TEM, FTIR, water vapor permeability, DSC and texture analyzer. The experimental findings show that Laponite has been dispersed uniformly

throughout the zein matrix, which is evident from the TEM images, FTIR spectra inspection as well as from the AFM roughness measurement. Films that were functionalized with the Laponite nanoparticles were found to be superior combining a relatively high resistance to tearing (150% increase in tensile strength) and stiffness (180% increase in Young’s modulus). The WVP of the films decreased 40% on addition of 10% nanoparticle. The findings in this study can benefit advanced materials research in many aspects as it thoroughly explores the underlying chemistry between zein and nanoparticles interaction and explains in detail the effect on their properties. This new and improved knowledge can lead to several innovative research opportunities related to enhancement of biodegradable packaging, designing of high-performance sensor materials and other biomaterials research with broad applications.

## Acknowledgements

The authors would like to thank Dr. Christopher Gilpin and Laurie Mueller for their assistance with TEM experiments, and Dr. Patricia Bishop and Dr. Hartmut Hedderich for their assistance with AFM and FTIR experiments. We would like to acknowledge USDA Hatch funds and the Scholle Endowment for financial support of this work.

## Compliance with ethical standards

**Conflict of interest** The authors would like to disclose that there are no conflicts of interests.

**Electronic supplementary material:** The online version of this article (<https://doi.org/10.1007/s10853-018-2061-6>) contains supplementary material, which is available to authorized users.

## References

- [1] Netravali AN, Chabba S (2003) Composites get greener. *Mater Today* 6:22–29. [https://doi.org/10.1016/S1369-7021\(03\)00427-9](https://doi.org/10.1016/S1369-7021(03)00427-9)
- [2] MacArthur E (2017) Beyond plastic waste. *Science* 358:843. <https://doi.org/10.1126/science.aao6749>
- [3] Law KL, Morét-Ferguson S, Maximenko NA et al (2010) Plastic accumulation in the North Atlantic subtropical Gyre. *Science* 329:1185–1188. <https://doi.org/10.1126/science.1192321>
- [4] Chen G-G, Qi X-M, Guan Y et al (2016) High strength hemicellulose-based nanocomposite film for food packaging applications. *ACS Sustain Chem Eng* 4:1985–1993. <https://doi.org/10.1021/acssuschemeng.5b01252>
- [5] Rouf TB, Kokini JL (2018) Natural biopolymer-based nanocomposite films for packaging applications. In: *Bio-nanocomposites for packaging applications*. Springer, Cham, pp 149–177
- [6] Lai H-M, Padua GW (1997) Properties and microstructure of plasticized zein films. *Cereal Chem J* 74:771–775. <https://doi.org/10.1094/CCHEM.1997.74.6.771>
- [7] Luecha J, Sozer N, Kokini JL (2010) Synthesis and properties of corn zein/montmorillonite nanocomposite films. *J Mater Sci* 45:3529–3537. <https://doi.org/10.1007/s10853-010-4395-6>
- [8] Luecha J, Hsiao A, Brodsky S et al (2011) Green microfluidic devices made of corn proteins. *Lab Chip* 11:3419–3425
- [9] Shukla R, Cheryan M (2001) Zein: the industrial protein from corn. *Ind Crops Prod* 13:171–192
- [10] Lawton JW (2002) Zein: a history of processing and use. *Cereal Chem J* 79:1–18. <https://doi.org/10.1094/CCHEM.2002.79.1.1>
- [11] Anderson TJ, Ilankovan P, Lamsal BP (2012) Two fraction extraction of  $\alpha$ -zein from DDGS and its characterization. *Ind Crops Prod* 37:466–472. <https://doi.org/10.1016/j.indcrop.2011.07.022>
- [12] Shi W, Dumont M-J (2013) Review: bio-based films from zein, keratin, pea, and rapeseed protein feedstocks. *J Mater Sci* 49:1915–1930. <https://doi.org/10.1007/s10853-013-7933-1>
- [13] Dashdorj U, Reyes MK, Unnithan AR et al (2015) Fabrication and characterization of electrospun zein/Ag nanocomposite mats for wound dressing applications. *Int J Biol Macromol* 80:1–7. <https://doi.org/10.1016/j.ijbiomac.2015.06.026>
- [14] Li J, Li Y, Lee T-C, Huang Q (2013) Structure and physical properties of zein/pluronic F127 composite films. *J Agric Food Chem* 61:1309–1318. <https://doi.org/10.1021/jf3043055>
- [15] Manisara P, Parichat M (2012) Cellulose microfibril from banana peels as a nanoreinforcing fillers for zein films. *Open J Polym Chem*. <https://doi.org/10.4236/ojpcem.2012.22007>
- [16] Oliviero M, Verdolotti L, Di Maio E et al (2011) Effect of supramolecular structures on thermoplastic zein-lignin bio-nanocomposites. *J Agric Food Chem* 59:10062–10070. <https://doi.org/10.1021/jf201728p>
- [17] Ozcalik O, Tihminlioglu F (2013) Barrier properties of corn zein nanocomposite coated polypropylene films for food packaging applications. *J Food Eng* 114:505–513. <https://doi.org/10.1016/j.jfoodeng.2012.09.005>
- [18] Nedi I, Di Maio E, Iannace S (2012) The role of protein–plasticizer–clay interactions on processing and properties of thermoplastic zein bionanocomposites. *J Appl Polym Sci* 125:E314–E323. <https://doi.org/10.1002/app.36860>
- [19] Gaharwar AK, Rivera CP, Wu C-J, Schmidt G (2011) Transparent, elastomeric and tough hydrogels from poly(ethylene glycol) and silicate nanoparticles. *Acta Biomater* 7:4139–4148. <https://doi.org/10.1016/j.actbio.2011.07.023>
- [20] Utech S, Boccaccini AR (2016) A review of hydrogel-based composites for biomedical applications: enhancement of hydrogel properties by addition of rigid inorganic fillers. *J Mater Sci* 51:271–310. <https://doi.org/10.1007/s10853-015-9382-5>
- [21] Kvien I, Sugiyama J, Votrubec M, Oksman K (2007) Characterization of starch based nanocomposites. *J Mater Sci* 42:8163–8171. <https://doi.org/10.1007/s10853-007-1699-2>

- [22] Liu F, Jiang G-C, Wang K, Wang J (2017) Laponite nanoparticle as a multi-functional additive in water-based drilling fluids. *J Mater Sci* 52:12266–12278. <https://doi.org/10.1007/s10853-017-1375-0>
- [23] Chouhan DK, Rath SK, Kumar A et al (2015) Structure-reinforcement correlation and chain dynamics in graphene oxide and Laponite-filled epoxy nanocomposites. *J Mater Sci* 50:7458–7472. <https://doi.org/10.1007/s10853-015-9305-5>
- [24] Li X, Zhou M, Xu H et al (2014) Synthesis and electrochemical performances of a novel two-dimensional nanocomposite: polyaniline-coated laponite nanosheets. *J Mater Sci* 49:6830–6837. <https://doi.org/10.1007/s10853-014-8385-y>
- [25] Wu W, Dong Z, He J et al (2016) Transparent cellulose/Laponite nanocomposite films. *J Mater Sci* 51:4125–4133. <https://doi.org/10.1007/s10853-016-9735-8>
- [26] Shan D, Li Q-B, Ding S-N et al (2010) Reagentless biosensor for hydrogen peroxide based on self-assembled films of horseradish peroxidase/laponite/chitosan and the primary investigation on the inhibitory effect by sulfide. *Biosens Bioelectron* 26:536–541. <https://doi.org/10.1016/j.bios.2010.07.051>
- [27] Zanini VP, López de Mishima B, Solís V (2011) An amperometric biosensor based on lactate oxidase immobilized in laponite–chitosan hydrogel on a glassy carbon electrode. Application to the analysis of l-lactate in food samples. *Sens Actuators B Chem* 155:75–80. <https://doi.org/10.1016/j.snb.2010.11.026>
- [28] Barbieri M, Cellini F, Cacciotti I et al (2017) In situ temperature sensing with fluorescent chitosan-coated PNI-PAAm/alginate beads. *J Mater Sci* 52:12506–12512. <https://doi.org/10.1007/s10853-017-1345-6>
- [29] Schmidt G, Nakatani AI, Butler PD, Han CC (2002) Small-angle neutron scattering from viscoelastic polymer-clay solutions. *Macromolecules* 35:4725–4732. <https://doi.org/10.1021/ma0115141>
- [30] Schmidt G, Nakatani AI, Butler PD et al (2000) Shear orientation of viscoelastic polymer-clay solutions probed by flow birefringence and SANS. *Macromolecules* 33:7219–7222. <https://doi.org/10.1021/ma9918811>
- [31] Gezer PG, Liu GL, Kokini JL (2016) Development of a biodegradable sensor platform from gold coated zein nanophotonic films to detect peanut allergen, Ara h1, using surface enhanced raman spectroscopy. *Talanta* 150:224–232. <https://doi.org/10.1016/j.talanta.2015.12.034>
- [32] Gezer PG, Hsiao A, Kokini JL, Liu GL (2016) Simultaneous transfer of noble metals and three-dimensional micro- and nanopatterns onto zein for fabrication of nanophotonic platforms. *J Mater Sci* 51:3806–3816. <https://doi.org/10.1007/s10853-015-9699-0>
- [33] Capello C, Fischer U, Hungerbühler K (2007) What is a green solvent? A comprehensive framework for the environmental assessment of solvents. *Green Chem* 9:927–934. <https://doi.org/10.1039/B617536H>
- [34] Panchapakesan C, Sozer N, Dogan H et al (2012) Effect of different fractions of zein on the mechanical and phase properties of zein films at nano-scale. *J Cereal Sci* 55:174–182. <https://doi.org/10.1016/j.jcs.2011.11.004>
- [35] Mejia CD, Mauer LJ, Hamaker BR (2007) Similarities and differences in secondary structure of viscoelastic polymers of maize  $\alpha$ -zein and wheat gluten proteins. *J Cereal Sci* 45:353–359. <https://doi.org/10.1016/j.jcs.2006.09.009>
- [36] Bal Ram Singh (1999) Basic aspects of the technique and applications of infrared spectroscopy of peptides and proteins. In: *Infrared analysis of peptides and proteins*. American Chemical Society, pp 2–37
- [37] ASTM E (96) Standard test methods for water vapor transmission of materials. Foundation drainage rate: Hydraulic Gradient 1:18
- [38] Gezer PG, Brodsky S, Hsiao A et al (2015) Modification of the hydrophilic/hydrophobic characteristic of zein film surfaces by contact with oxygen plasma treated PDMS and oleic acid content. *Colloids Surf B* 135:433–440. <https://doi.org/10.1016/j.colsurfb.2015.07.006>
- [39] Testing AS for Materials (2010) Standard test method for tensile properties of thin plastic sheeting. ASTM International
- [40] Guimarães TR, de Camargo Chaparro T, D’Agosto F et al (2014) Synthesis of multi-hollow clay-armored latexes by surfactant-free emulsion polymerization of styrene mediated by poly(ethylene oxide)-based macroRAFT/Laponite complexes. *Polym Chem* 5:6611–6622. <https://doi.org/10.1039/C4PY00362D>
- [41] Lewandowska K, Sionkowska A, Kaczmarek B, Furtos G (2014) Mechanical and morphological studies of chitosan/clay composites. *Mol Cryst Liq Cryst* 590:193–198. <https://doi.org/10.1080/15421406.2013.874718>
- [42] Fatnassi M, Solterbeck C-H, Es-Souni M (2014) Clay nanomaterial thin film electrodes for electrochemical energy storage applications. *RSC Adv* 4:46976–46979. <https://doi.org/10.1039/C4RA04330H>
- [43] Hodges CS, Ding Y, Biggs S (2010) The influence of nanoparticle shape on the drying of colloidal suspensions. *J Colloid Interface Sci* 352:99–106. <https://doi.org/10.1016/j.jcis.2010.08.044>
- [44] Shan D, Wang Y-N, Xue H-G et al (2009) Xanthine oxidase/laponite nanoparticles immobilized on glassy carbon electrode: direct electron transfer and multielectrocatalysis.

- Biosens Bioelectron 24:3556–3561. <https://doi.org/10.1016/j.bios.2009.05.009>
- [45] Shi K, Kokini JL, Huang Q (2009) Engineering zein films with controlled surface morphology and hydrophilicity. *J Agric Food Chem* 57:2186–2192. <https://doi.org/10.1021/jf803559v>
- [46] Lee H-T, Lin L-H (2006) Waterborne polyurethane/clay nanocomposites: novel effects of the clay and its interlayer ions on the morphology and physical and electrical properties. *Macromolecules* 39:6133–6141. <https://doi.org/10.1021/ma060621y>
- [47] Farmahini-Farahani M, Khan A, Lu P et al (2017) Surface morphological analysis and water vapor barrier properties of modified Cloisite 30B/poly(3-hydroxybutyrate-co-3-hydroxyvalerate) composites. *Appl Clay Sci* 135:27–34. <https://doi.org/10.1016/j.clay.2016.08.033>
- [48] Lin-Vien D, Colthup NB, Fateley WG, Grasselli JG (1991) The handbook of infrared and Raman characteristic frequencies of organic molecules. Elsevier, New York
- [49] Yamazaki H, Ishikawa Y, Fujii M et al (2014) The influence of fluorinated silicon nitride gate insulator on positive bias stability toward highly reliable amorphous InGaZnO thin-film transistors. *ECS J Solid State Sci Technol* 3:Q20–Q23. <https://doi.org/10.1149/2.014402jss>
- [50] Reza Mahdavinia G, Ettehad S, Amini M, Sabzi M (2015) Synthesis and characterization of hydroxypropyl methylcellulose-g-poly(acrylamide)/LAPONITE® RD nanocomposites as novel magnetic- and pH-sensitive carriers for controlled drug release. *RSC Adv* 5:44516–44523. <https://doi.org/10.1039/C5RA03731J>
- [51] Krimm S, Bandekar J (1986) Vibrational spectroscopy and conformation of peptides, polypeptides, and proteins. *Adv Protein Chem* 38:181–364. [https://doi.org/10.1016/S0065-3233\(08\)60528-8](https://doi.org/10.1016/S0065-3233(08)60528-8)
- [52] Mizutani Y, Matsumura Y, Imamura K et al (2003) Effects of water activity and lipid addition on secondary structure of zein in powder systems. *J Agric Food Chem* 51:229–235. <https://doi.org/10.1021/jf0205007>
- [53] Matsushima N, Danno G, Takezawa H, Izumi Y (1997) Three-dimensional structure of maize alpha-zein proteins studied by small-angle X-ray scattering. *Biochim Biophys Acta-Protein Struct Mol Enzym* 1339:14–22. [https://doi.org/10.1016/S0167-4838\(96\)00212-9](https://doi.org/10.1016/S0167-4838(96)00212-9)
- [54] Benami A, Santana G, Ortiz A et al (2007) Strong white and blue photoluminescence from silicon nanocrystals in SiN<sub>x</sub> grown by remote PECVD using SiCl<sub>4</sub>/NH<sub>3</sub>. *Nanotechnology* 18:155704. <https://doi.org/10.1088/0957-4484/18/15/155704>
- [55] Li Y, Wang L, Yin S et al (2011) Rapid crystallization process of amorphous silicon nitride. *J Am Ceram Soc* 94:4169–4173. <https://doi.org/10.1111/j.1551-2916.2011.04914.x>
- [56] Kopani M, Mikula M, Pinčík E et al (2014) FT IR spectroscopy of nitric acid oxidation of silicon with hafnium oxide very thin layer. *Appl Surf Sci* 301:24–27. <https://doi.org/10.1016/j.apsusc.2014.01.124>
- [57] Pluchery O, Costantini J-M (2012) Infrared spectroscopy characterization of 3C–SiC epitaxial layers on silicon. *J Phys D Appl Phys* 45:495101. <https://doi.org/10.1088/0022-3727/45/49/495101>
- [58] Huang X, Brittain WJ (2001) Synthesis and characterization of PMMA nanocomposites by suspension and emulsion polymerization. *Macromolecules* 34:3255–3260. <https://doi.org/10.1021/ma001670s>
- [59] Rouf TB, Kokini JL (2016) Biodegradable biopolymer–graphene nanocomposites. *J Mater Sci* 51:9915–9945. <https://doi.org/10.1007/s10853-016-0238-4>
- [60] Peles Z, Zilberman M (2012) Novel soy protein wound dressings with controlled antibiotic release: mechanical and physical properties. *Acta Biomater* 8:209–217. <https://doi.org/10.1016/j.actbio.2011.08.022>
- [61] Martin-Polo M, Mauguin C, Voilley A (1992) Hydrophobic films and their efficiency against moisture transfer. 1. Influence of the film preparation technique. *J Agric Food Chem* 40:407–412
- [62] Martin-Polo M, Voilley A, Blond G et al (1992) Hydrophobic films and their efficiency against moisture transfer. 2. Influence of the physical state. *J Agric Food Chem* 40:413–418
- [63] Bras J, Vaca-Garcia C, Borredon M-E, Glasser W (2007) Oxygen and water vapor permeability of fully substituted long chain cellulose esters (LCCE). *Cellulose* 14:367–374. <https://doi.org/10.1007/s10570-007-9123-2>
- [64] Hirvikorpi T, Vähä-Nissi M, Harlin A et al (2011) Enhanced water vapor barrier properties for biopolymer films by polyelectrolyte multilayer and atomic layer deposited Al<sub>2</sub>O<sub>3</sub> double-coating. *Appl Surf Sci* 257:9451–9454. <https://doi.org/10.1016/j.apsusc.2011.06.031>
- [65] Tunç S, Duman O, Polat TG (2016) Effects of montmorillonite on properties of methyl cellulose/carvacrol based active antimicrobial nanocomposites. *Carbohydr Polym* 150:259–268. <https://doi.org/10.1016/j.carbpol.2016.05.019>
- [66] Mahmoudian S, Wahit MU, Ismail AF, Yussuf AA (2012) Preparation of regenerated cellulose/montmorillonite nanocomposite films via ionic liquids. *Carbohydr Polym* 88:1251–1257. <https://doi.org/10.1016/j.carbpol.2012.01.088>